JPE 19-1-17

https://doi.org/10.6113/JPE.2019.19.1.179
ISSN(Print): 1598-2092 / ISSN(Online): 2093-4718

Predictive Current Control of Four-Quadrant Converters Based on Specific Sampling Method and Modified Z-Transform

Gang Zhang†, Jianglin Qian*, Zhigang Liu**, and Zhongbei Tian***

†School of Electrical Engineering, Beijing Jiaotong University, Beijing, China
*CRRC Zhuzhou Locomotive Co., Ltd., Hunan, China
**Beijing Electrical Engineering Technology Research Center, Beijing, China
***Birmingham Centre for Railway Research and Education, Department of Electronic, Electrical and Systems Engineering, University of Birmingham, Birmingham, ENG, UK

Abstract

Four-quadrant converters (4QCs) are widely used as AC-DC power conversion interfaces in many areas. A control delay commonly exists in the digital implementation process of 4QCs, especially for high power 4QCs with a low switching frequency. This usually results in alternating current distortion, increased current harmonic content and system instability. In this paper, the control delay is divided into a computation delay and a PWM delay. The impact of the control delay on the performance of a 4QC is briefly analyzed. To obtain a fundamental value of AC current that is as accurately as possible, a specific sampling method considering the PWM pattern is introduced. Then a current predictive control based on a modified z-transform is proposed, which is effective in reducing the control delay and easy in terms of digital implementation. In addition, it does not depend on object models and parameters. The feasibility and effectiveness of the proposed predictive current control method is verified by simulation and experimental results.

Key words: AC-DC power conversion, Current control, Digital control, Predictive control, PWM converter

I. INTRODUCTION

Four-quadrant converters (4QCs) are widely employed in various application fields such as wind power generation, solar power generation, smart microgrids, rail transit systems and so on [1]-[4]. As the power conversion interface between the motor inverter and the overhead line, the 4QCs in electric multiple units (EMU) carry out the role of bidirectional energy conversion, unit power factor control and DC voltage regulation [5], [6]. In order to achieve higher speeds, the power capacity of a 4QC should be increased. However, due to the switching losses constraint of high-voltage and high-power IGBT devices, the switching frequency of the 4QC in an EMU must be as low as possible (about 500Hz).

In the conventional control method of 4QCs, the sampling and calculating frequency is usually consistent with the switching frequency (f_s). The sampling and calculating are executed at the beginning of each carrier period, while the duty ratio can only be updated at the beginning of the next carrier period [7]. Thus, a lower switching frequency leads to a greater control delay. This results in deteriorated performance of the current control, which can lead to unstable operation of the system [8]. In order to simplify the expression, the control delay is divided into two parts in this paper: the computation delay and the PWM delay. The computation delay includes the AD sampling delay, filtering delay and algorithm execution delay.

Predictive current control is employed as a kind of effective method to compensate the computation delay [9]-[11]. A linear

Manuscript received Dec. 22, 2017; accepted Jul. 23, 2018
Recommended for publication by Associate Editor Sung-Jin Choi.
†Corresponding Author: gzhang@bjtu.edu.cn
Tel: +86-10-51687082, Fax: +86-10-51684032, Beijing Jiaotong Univ.
*CRRC Zhuzhou Locomotive Co., Ltd., China
**Beijing Electrical Engineering Technology Research Center, China
***Birmingham Centre for Railway Research and Education, Dept. of Electron., Electr. and Systems Eng., Univ. of Birmingham, ENG, UK

prediction method is introduced to compensate the computation delay and to increase the bandwidth of the controller in [9]. However, an extra correction for the prediction results is needed to improve accuracy. Smith prediction is proposed in [10], which can effectively compensate computation delay. However, a lot of computing resources are consumed. Kalman prediction is adopted in [11]. An adaptive Kalman filter is used to complete the prediction one-step ahead, which eliminates the delays in the system. In [9]-[11], future information is predicted based on past information and system models, where the prediction results are sensitive to the system models and parameters. An on-time prediction method based on an extended-state observer (ESO) is presented to reduce the side-effect of the model inaccuracy and parameter perturbation in [12]. However, it is relatively complex in terms of implementation.

Another way to reduce the computation delay is to change the AD sampling pattern. This reduces the computation delay to a certain extent by shifting the sampling instant as closely as possible to the PWM reference update instant [13]-[15]. However, since execution of the control algorithm always takes time, this method can reduce the computation delay but cannot completely eliminate it. In addition, this method makes the sampling point deviate from the fundamental wave, which can result in aliasing of the sampled signals, increase the sampling error and deteriorate the grid current waveform quality.

Multi-sampling techniques have also been used to reduce computation delay [16]-[19]. However, there are still some problems due to the disturbances of switching noise. The authors of [17] state that multi-sampling techniques can inject a high frequency disturbance into the feedback loop, which triggers nonlinear phenomena. Therefore, a dedicated filter is proposed to filter out interference and harmonics. However, a phase delay is inevitably introduced, which makes the multi-sampling solution lose some possible advantages. In order to suppress the low-order harmonic disturbance in the sampling data, a filter based on moving-average and anti-aliasing is employed in [18], [19]. However, to reduce the side-effect of the time delay introduced by the filter, the conventional current controller must be improved, which makes the control algorithm complicated.

Studies on removing the PWM delay have been carried out in [20]-[22]. The PWM delay is mainly determined by the PWM method. For general SPWM, the PWM reference is only updated at the trough of the carrier. In other words, it is updated once per switching cycle (T_{sw}), and is then kept constant. Thus, the PWM delay is $0.5T_{sw}$. Considering the single-phase 4QC applied in EMU, unipolar asymmetrical SPWM is adopted. The PWM reference is updated twice per switching cycle. This is done at the peak and trough point of the carrier. The PWM delay can be reduced to $0.25T_{sw}$. A novel PWM method has been proposed to reduce PWM delay in [23]. The PWM reference is updated N times per switching cycle, where the PWM delay is reduced to 1/N. However, this method can result in troublesome problems in terms of "multiple-comparation" or "pulses lost", which do not exist in conventional SPWM.

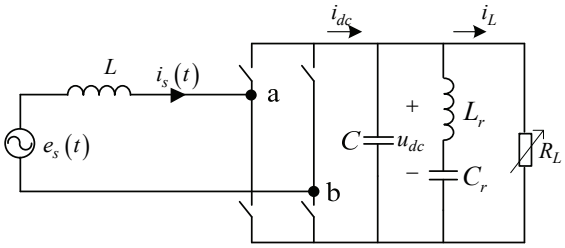

Fig. 1. Main circuit of a single phase 4QC.

For industrial applications, it is desirable to maintain a simple control concept [10]. This is also true for the digital implementation of a 4QC in an EMU. This paper focuses on solutions to reduce the control delay of a 4QC with a low switching frequency. This paper is organized as follows. The basic principle and control method of the 4QC are presented in section II. The influence of a control delay on the control stability and dynamic performance of a 4QC is analyzed in section III. A new predictive current control technique based on a special sampling method and a modified z-transform is proposed in section IV. In sections V and VI, the feasibility and effectiveness of the proposed predictive control are verified by simulation and experimental results.

II. Basic Principle and Control Method

The main circuit of a single phase 4QC used in an EMU is shown in Fig. 1. A SPWM method based on unipolar asymmetrical modulation is usually adopted.

First of all, the unipolar two-valued logic switch function S_k is defined by Equ. (1).

$$s_k = \begin{cases} 1 \\ 0 \end{cases} \quad (k = a, b) \tag{1}$$

Thus, the AC side voltage u_{ab} can be expressed by:

$$u_{ab}(t) = (s_a - s_b)u_{dc} \tag{2}$$

According to the main circuit shown in Fig.1, the inductance voltage u_L can be obtained using the KVL Law as:

$$u_L(t) = e_s - u_{ab} = e_s - (s_a - s_b)u_{dc} \tag{3}$$

Then the AC current i_s can be written as:

$$i_s(t) = \frac{1}{L}\int [e_s - (s_a - s_b)u_{dc}]dt \tag{4}$$

On the basis of the above relations, the amplitude and phase of the AC current i_s can be controlled by adjusting the amplitude and phase of the AC side voltage u_{ab}. In order to achieve independent control of the active and reactive power,

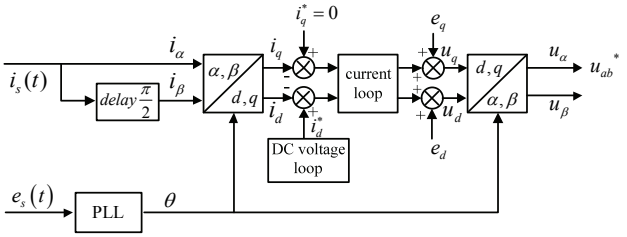

Fig. 2. Block diagram of a double loop control strategy based on the *dq* reference frame.

a double loop control strategy based on the *dq* reference frame is used in this paper [3], as shown in Fig. 2.

The feed-forward decoupling control strategy is adopted in the inner current loop. Then the control output in the *dq* coordinate system can be given by Eqs. (5)-(6).

$$u_d = -(K_{iP} + \frac{K_{iI}}{s})(i_d^* - i_d) + \omega L i_q + e_d \tag{5}$$

$$u_q = -(K_{iP} + \frac{K_{iI}}{s})(i_q^* - i_q) - \omega L i_d + e_q \tag{6}$$

III. Control Delay and its Influence Analysis

A. Computation Delay

In the control of a single phase 4QC, the PWM reference is usually updated at the peak and trough points of the PWM carrier as shown in Fig. 3. u_c(t) is the carrier, u_{ab}^*(t) is the PWM reference, and i_s(t) is the AC current of the 4QC. (n,m) is a sampling instant between instant n-1 and instant n, and *m* is a coefficient, which can be used to describe the length of the time from instant n-1 to instant (n,m), where $0 \le m \le 1$. $i_s(n,m)$ is the AD sampling value that is obtained at the instant (n,m), and will be used to calculate $u_{ab}(n)$. The time duration between the instant of the AD sampling and the instant of the PWM reference updating is called the computation delay T_d. It can be seen in Fig. 3 that $T_d=\lambda T_s=(1-m)T_s$, where λ is called the delay coefficient and $0 \le \lambda \le 1$. T_s is the control period.

For the conventional control method, the current sampling frequency is usually the same as the control frequency. The AC current is sampled at the peak and trough of the PWM carrier to avoid switching noise and to leave enough time for sampling and calculating, which means that m=0, λ=1 and $T_d=T_s$. However, this results in a long computation delay.

B. PWM Delay

The PWM delay is the duration time between the instant when the PWM reference is updated and the instant when the equivalent output waveform is generated. Taking asymmetric regular sampling as an example, the value of the PWM reference is updated at the peaks and troughs of the carrier, as shown in Fig. 4. u_{ab}(t) is the expected reference. u_{ab_hold}(t) is

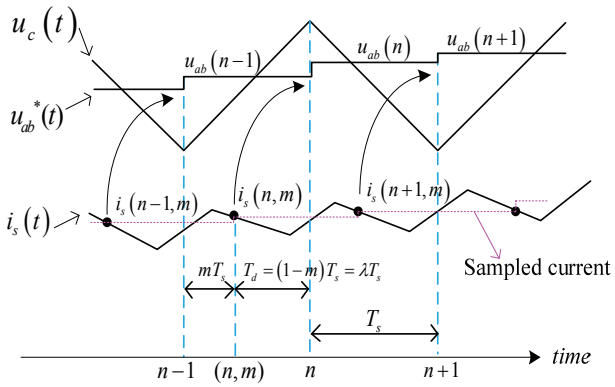

Fig. 3. Computation delay of the conventional control method.

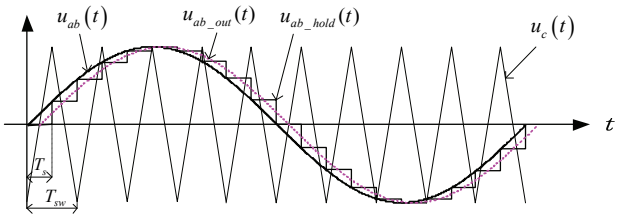

Fig. 4. Schematic of the PWM delay.

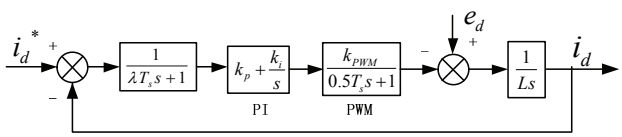

Fig. 5. Block diagram of the i_d current loop.

the actual PWM reference based on the zero-order hold, which is directly compared with the triangle carrier and generates pulses to control the IGBT switches. u_{ab_out}(t) is the equivalent output waveform.

The control (sampling and calculating) period T_s is half of the carrier period T_{sw}. It can be seen from Fig. 4 that there is half a control period delay ($0.5T_s$) between u_{ab}(t) and u_{ab_out}(t). The PWM process of the 4QC can be considered as a first-order inertial link (also called a first-order lag link), which is used to describe the system with some inertia and a fixed time delay.

C. Influence Analysis of the Control Delay

According to the control strategy in Fig. 2, a block diagram of the inner current loop is shown in Fig. 5, which considers both the computation delay and the PWM delay. Taking the decoupled active current i_d as an example, $1/(\lambda T_s s+1)$ is the computation delay, where λ is the delay coefficient, and $k_{PWM}/(0.5T_s s+1)$ is the PWM delay, where k_{PWM} is the equivalent gain of the H bridge.

In order to simplify the analysis, the disturbance of e_d is not considered, and the transfer function of the PI regulator is written in the zero pole form, as shown in Equ. (7).

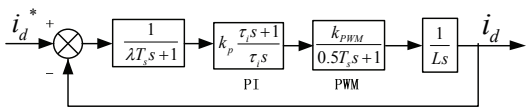

Fig. 6. Simplified block diagram of the i_d current loop without e_d.

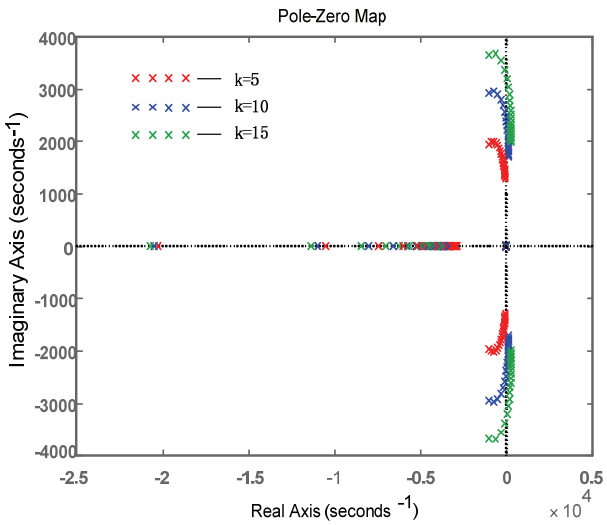

Fig. 7. Closed-loop pole distribution with the delay coefficient λ.

$$k_p+\frac{k_i}{s}=k_p\frac{\tau_i s+1}{\tau_i s}\qquad k_i=\frac{k_p}{\tau_i} \tag{7}$$

The simplified structure of the i_d current loop without e_d can be obtained, as shown in Fig. 6.

In Fig. 6, the open-loop transfer function of the current loop can be written as:

$$\begin{aligned}W_{oi}(s)&=\frac{k_p k_{PWM}(\tau_i s+1)}{L\tau_i s^2(\lambda T_s s+1)(0.5T_s s+1)}\\&=\frac{k_p k_{PWM}(\tau_i s+1)}{0.5\lambda L\tau_i T_s^2 s^4+(0.5+\lambda)L\tau_i T_s s^3+L\tau_i s^2}\end{aligned} \tag{8}$$

The closed-loop transfer function can be obtained as:

$$\begin{aligned}W_{ci}(s)&=\frac{W_{oi}(s)}{1+W_{oi}(s)}=\frac{k_p k_{PWM}(\tau_i s+1)}{L\tau_i s^2(\lambda T_s s+1)(0.5T_s s+1)+k_p k_{PWM}(\tau_i s+1)}\\&=\frac{k_p k_{PWM}(\tau_i s+1)}{0.5\lambda L\tau_i T_s^2 s^4+(0.5+\lambda)L\tau_i T_s s^3+L\tau_i s^2+k_p k_{PWM}\tau_i s+k_p k_{PWM}}\end{aligned} \tag{9}$$

In order to analyze the influence of different computation delays λT_s on the system stability, the closed-loop pole distribution with the delay coefficient λ as the variable can be plotted according to the closed-loop transfer function in Equ. (9). The pole distribution when the closed-loop gains k (where, $k=k_p k_{PWM}$) of the current loop are 5, 10 and 15 is shown in Fig. 7.

Fig. 8 shows an enlarged diagram of the dominant pole area of Fig. 7, where the following parameters have been employed: AC filter inductance L=2.08mH, switching frequency f_{sw}=500Hz, and $\tau_i=k_p/k_i=1$.

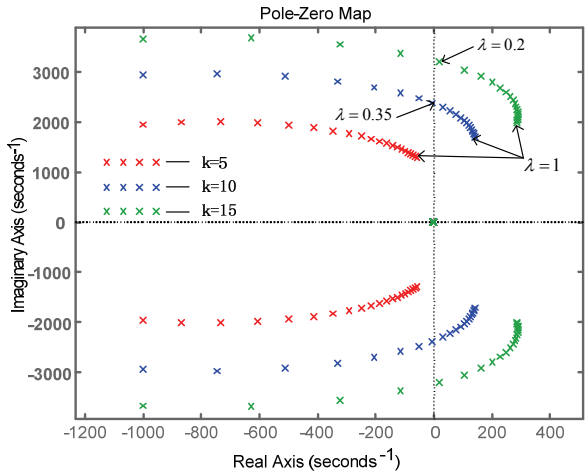

Fig. 8. Enlarged diagram of the dominant pole area.

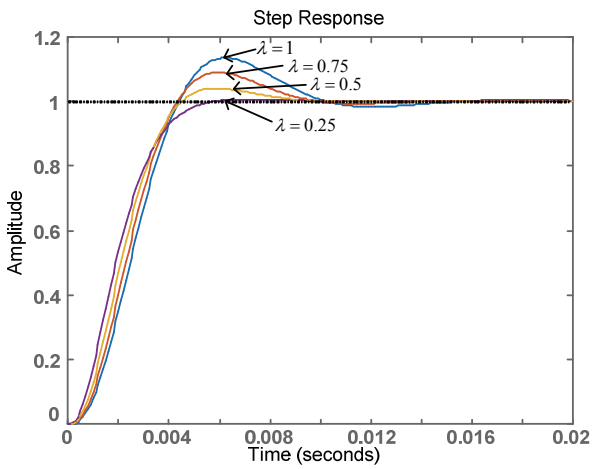

Fig. 9. Step response of the current loop under different λ.

A number of things can be found from Fig. 8. When k=5 and λ varies from 0 to 1, the closed-loop all of the dominant poles of the system are distributed in the left half plane of the s plane, and the system is in a stable state. When k=10 and λ varies from 0 to 0.35, the dominant poles of the system are distributed in the left half plane of the s plane, and when λ varies from 0.35 to 1, the dominant poles of the system are distributed in the right half plane of the s plane, which indicates that the system is unstable. When k=15 and λ varies from 0 to 0.2, the dominant poles of the system are distributed in the left half plane of the s plane, and when λ varies from 0.2 to 1, the dominant poles of the system are distributed in the right half plane of the s plane, which also indicates that the system is unstable. According to the above analysis, it can be concluded that with an increase of the computation delay, the stability of the system gets worse. The range of the closed-loop gain has to be smaller to ensure the stability of the system.

In order to analyze the influence of different computation delays on the dynamic performance of the system, step response curves are drawn according to Equ. (9) when k=1

and λ varies from 0.25 to 1, as shown in Fig. 9. It can be found from Fig. 9 that with an increase of the computation delay, the dynamic response speed of the current loop becomes slower, the regulation time becomes longer, and the overshoot becomes larger. Therefore, the computation delay should be as small as possible for the control system.

IV. Predictive Current Control Based on the Specific Sampling Method and the Modified Z-Transform

A. Specific Sampling Method

The specific sampling method aims to acquire the fundamental value of AC current as accurately as possible without the impact of high frequency noise components. According to Eqs. (2)-(4), the interrelation between the AC current $i_s(t)$ and the triangular carrier $u_c(t)$ under unipolar asymmetry SPWM can be obtained, as shown in Fig. 10.

In Fig. 10, $u_{ab}^*(t)$, which is calculated by the digital controller, is used as a PWM reference of the left half-bridge A, while $-u_{ab}^*(t)$ is used as a PWM reference of the right half-bridge B. By comparing $u_{ab}^*(t)$ and $-u_{ab}^*(t)$ in the same triangular carrier, the switching function S_a、S_b of the two half-bridges are obtained, which can be used to control the switches of the A and B half-bridges, respectively. Then the waveform of $u_{ab}(t)$ is obtained from Equ. (2) as shown in Fig. 10. According to Equ. (3), the waveform of the inductance voltage $u_L(t)$ can be drawn (assuming that e_s and u_{dc} are kept constant in a switching period). A waveform of the AC current $i_s(t)$ can be obtained from Equation (4), as shown in Fig. 10.

Fig. 10 shows that when unipolar asymmetry SPWM modulation is adopted, the AC current waveform consists of several segments with positive (or negative) slopes. Research shows that the midpoint value of each segment is closest to the fundamental value of the AC current. In addition, the midpoint of each segment corresponds to the peak, trough, and two waists of the triangular carrier, respectively. Therefore, a specific sampling method is proposed in this paper.

For the specific sampling method, the current sampling frequency is twice the control period T_s. Besides the peaks and troughs, the midpoints of the two waists of the carrier are selected as sampling instants. Choosing midpoints, that is to say m=0.5, makes sure that $i_s(n,m)$ is the fundamental value of the current. The sampling sequence $\delta_{AD}(t)$ is shown in Fig. 11.

B. Modified z-Transform Theory

The predictive current control proposed in this paper is mainly based on the modified z-transform theory. The modified z-transform is also known as the advanced z-transform, it is an extension of the z-transform [24]. The modified z-transform has information of the system at the sampling point, along with information of the continuous

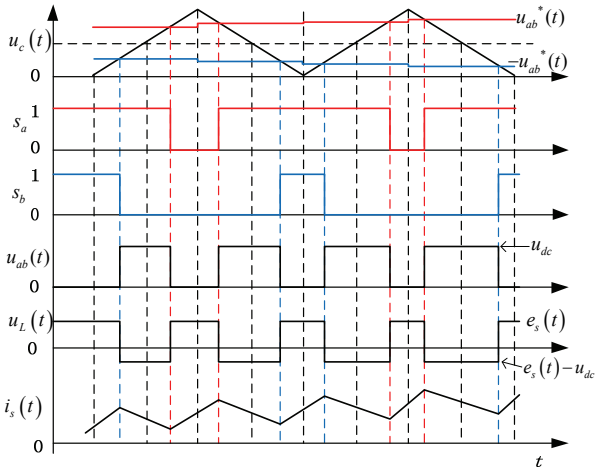

Fig. 10. Waveforms under the unipolar asymmetry SPWM.

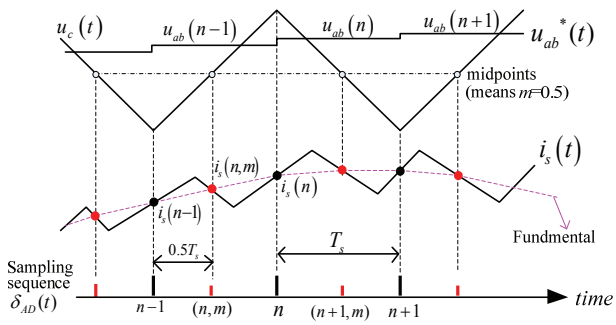

Fig. 11. Proposed specific sampling method (m=0.5).

function between the sampling points [25]. The modified z-transform of the continuous signal $f(t)$ is defined as the z-transform of the delayed signal $f(t-\lambda T_s)$ as shown in Equ. (10), where $0<\lambda<1$.

$$\begin{aligned} F(z,m) &= Z\left[f\left(t-\lambda T_s\right)\right] \\ &= \sum_{k=0}^{\infty} f(kT_s-\lambda T_s)\, z^{-k} \end{aligned} \tag{10}$$

Given that $m=1-\lambda$, Equ. (10) can be written as:

$$\begin{aligned} F(z,m) &= z^{-1}\, Z\left[f\left(kT_s+mT_s\right)\right] \\ &= z^{-1} \sum_{k=0}^{\infty} f(kT_s+mT_s)\, z^{-k} \end{aligned} \tag{11}$$

Since the specific sampling method used in this paper can sample the fundamental component of the AC current, the AC current model can be considered as a sine or cosine function. Thus, the AC current can be expressed as:

$$i_s(t)=\sin\omega t,\quad \omega=2\pi f=100\pi \tag{12}$$

Finally, the modified z-transform of the current can be expressed as:

$$I_s(z,m)=\frac{z\sin m\omega T_s+\sin(1-m)\omega T_s}{z^2-2z\cos\omega T_s+1} \tag{13}$$

C. Predictive Current Control

The z-transform of Equ. (12) is written in Equ. (14).

$$I_s(z)=\frac{z\sin\omega T_s}{z^2-2z\cos\omega T_s+1} \tag{14}$$

The relationship between $I_s(z)$ and $I_s(z,m)$ can be obtained in Equ. (15) by solving Equs. (13)-(14).

$$\begin{aligned} I_s(z,m)&=\frac{z\sin m\omega T_s+\sin(1-m)\omega T_s}{z\sin\omega T_s}I_s(z)\\ &=\frac{\sin m\omega T_s}{\sin\omega T_s}I_s(z)+\frac{\sin(1-m)\omega T_s}{\sin\omega T_s}z^{-1}I_s(z)\end{aligned} \tag{15}$$

For the sake of simplicity:

$$\begin{cases} A=\dfrac{\sin m\omega T_s}{\sin\omega T_s}\\ B=\dfrac{\sin(1-m)\omega T_s}{\sin\omega T_s}\end{cases} \tag{16}$$

Then Equ. (15) can be written as Equ. (17).

$$I_s(z,m)=AI_s(z)+BI_s(z-1) \tag{17}$$

Solving Equ. (17) yields:

$$I_s(z)=\frac{1}{A}I_s(z,m)-\frac{B}{A}I_s(z-1) \tag{18}$$

The current prediction equation can be obtained as (19).

$$\hat{i}_s(n)=\frac{1}{A}i_s(n,m)-\frac{B}{A}i_s(n-1) \tag{19}$$

i_s(n,m) and i_s(n-1) in Equ. (19) are shown in Fig. 11. When i_s(n,m) is obtained, Equ. (19) can be used to predict the current value $\hat{i}_s(n)$. Then $\hat{i}_s(n)$ can be used in the current closed-loop control, as a real-time current feedback value.

According to the block diagram in Fig. 5, the zero-order holder effect of the PWM link can be expressed by I_s(s)/V_L(s) as Equ. (20).

$$\frac{I_s(s)}{V_L(s)}=g(s)=\frac{1-e^{-T_s s}}{s}\frac{1}{Ls} \tag{20}$$

The transfer function by the z-transform is calculated as (21), where K_b=T_S/L.

$$\frac{I_s(z)}{V_L(z)}=g(z)=\frac{T_s}{L}\frac{1}{z-1}=\frac{K_b}{z-1} \tag{21}$$

According to Equs. (19)-(21), a block diagram of the predictive current control based on the modified z-transform is shown in Fig. 12.

The above current prediction algorithm is applied to the control scheme under the *dq* synchronous rotating coordinate system [26]. Then the complete control scheme of the 4QC is so shown in Fig. 13. In principle, the AC grid voltage e_s(t) should adopt the same prediction algorithm to make sure that the i_s and e_s used in the control scheme are at the same instant.

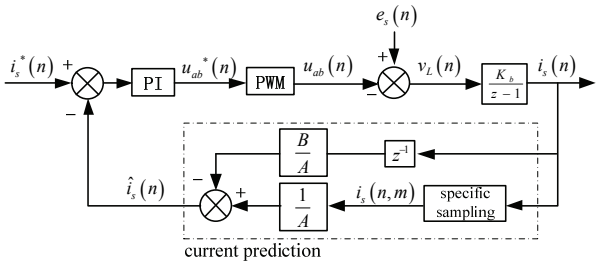

Fig. 12. Control block diagram of the predictive current control.

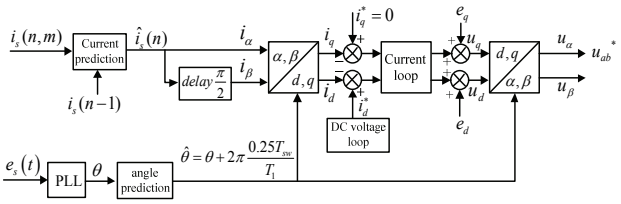

Fig. 13. Proposed predictive current control scheme based on the *dq* reference frame.

However, for the sake of simplicity, an angle prediction method is introduced, which compensates the angle delay and make the 4QC obtain a unify factor. The predicted angle is calculated as Equ. (21), where T_1 is the period of a fundamental wave.

$$\hat{\theta}=\theta+2\pi\frac{0.25T_{sw}}{T_1} \tag{21}$$

V. Simulation Analysis

A simulation model is built with MATLAB/Simulink according to the main circuit of the 4QC shown in Fig. 1. The parameters of the 4QC used in the simulation are shown in Table I. The simulation step is set to 10μs, and the simulation duration is 3s. The load is increased from 0% to 50% at 0.5s, and to 100% at 1.5s.

In order to compare the performances of different control methods, three control methods have been implemented in this paper, including two conventional methods CM1 and CM2, and the proposed predictive current control as shown in Table II. The computation delays of CM1 and CM2 are T_s and $0.5T_s$, respectively. The computation delay of the predictive control is close to zero in theory.

A. Two Conventional Control Methods

In order to compare them with the predictive current control, the two conventional control methods are simulated firstly. Fig. 14(a) and Fig. 14(b) are AC side waveforms when T_d=T_s and T_d=$0.5T_s$, respectively. The closed-loop control parameters (e.g. k_p, k_i) are kept the same. e_s is the AC grid voltage and i_s is the AC current of the 4QC. It can be seen from Fig. 14(a) that when T_d=T_s, regardless of whether it is under the half-load or full-load condition, the AC current waveform has a large overall fluctuation. There are remarkable

TABLE I
PARAMETERS OF THE 4QC

Items	value
DC rated voltage u_{dc}	1500V
Converter rated power P	460kW
AC Filter inductance L	2.08mH
AC rated voltage e_s	900Vrms
AC Rated current i_s	511Arms
Resonant inductance L_r	3.59mH
Resonant capacitor C_r	7.06mF
DC capacitor C	4mF
Load resistance R_L	4.9 Ω
Switching frequency f_{sw}	500Hz

TABLE II
THREE CONTROL METHODS

control method	current sampling instant relative to carrier	PWM reference update instant	delay / T_d
CM1	trough	peak	T_s
	peak	trough	T_s
CM2	midpoint of up-slope	peak	$0.5T_s$
	midpoint of down-slope	trough	$0.5T_s$
predictive control	trough and midpoint of up-slope	peak	0
	peak and midpoint of down-slope	trough	0

distortions in the enlarged waveforms. It can be seen from Fig. 14(b) that when T_d=0.5T_s, the AC current waveform becomes more stable, and the AC current quality is improved to some extent. However, obvious distortion can be found in the enlarged waveform.

B. Predictive Current Control

The predictive current control scheme in the *dq* rotating coordinate system shown in Fig. 13 is also verified by simulation results. Fig. 15 shows waveforms of the AC current i_s and AC voltage e_s under different load conditions when the proposed predictive current control scheme is adopted. It can be seen from Fig. 15 that the AC current waveform becomes a lot more sinusoidal under half-load and full-load conditions.

Fig. 16 shows AC current waveforms in a fundamental period. The red waveform is the actual AC current, the blue waveform is the AD sampling value, the green waveform is the predicted value, and the purple waveform is the triangular carrier. Through the previous two sampling values i_s(n-1) and i_s(n,m), the next value of the AC current $\hat{i}_s(n)$ is predicted and used to participate in the current loop control. The simulation results show that the predicted current value $\hat{i}_s(n)$ is very close to the next actual sampling current value i_s(n), where the purpose of the current prediction is accomplished.

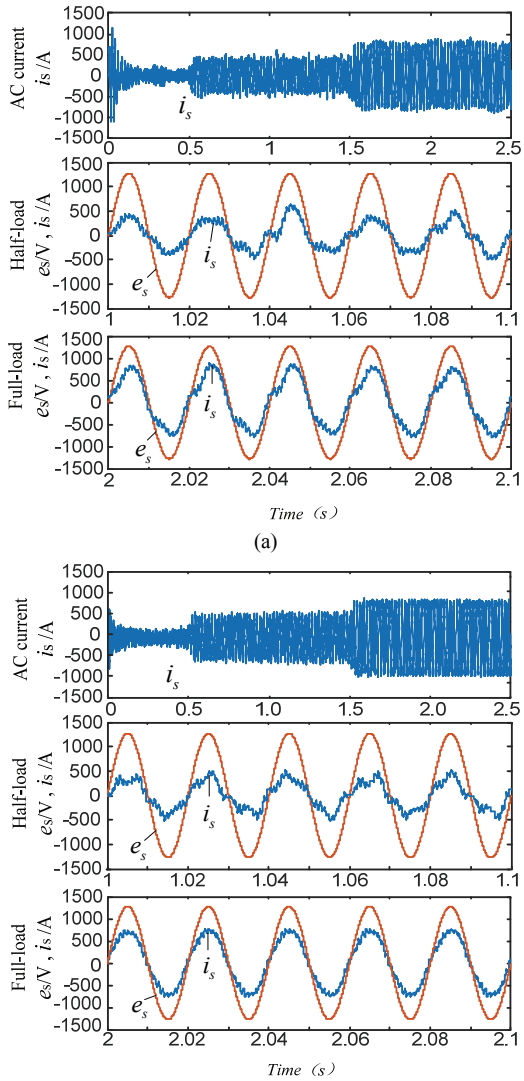

Fig. 14. AC side waveforms of the two conventional control methods: (a)T_d=T_s; (b) T_d=0.5T_s.

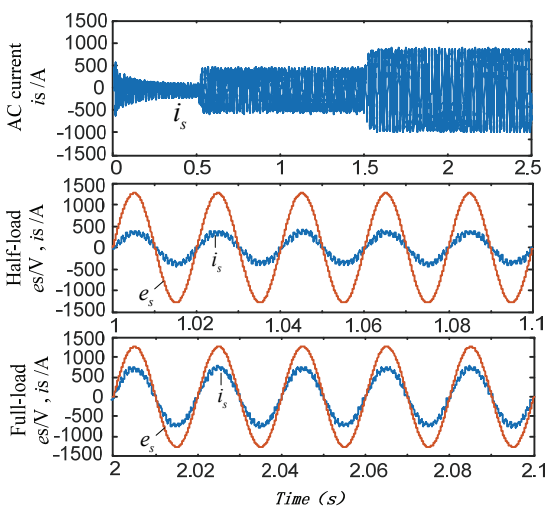

Fig. 15. AC current waveforms under the proposed predictive current control.

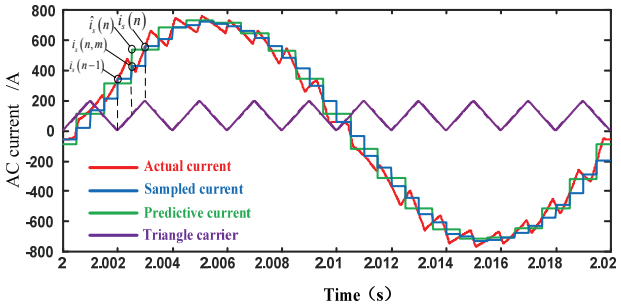

Fig. 16. AC current waveforms under the predictive current control.

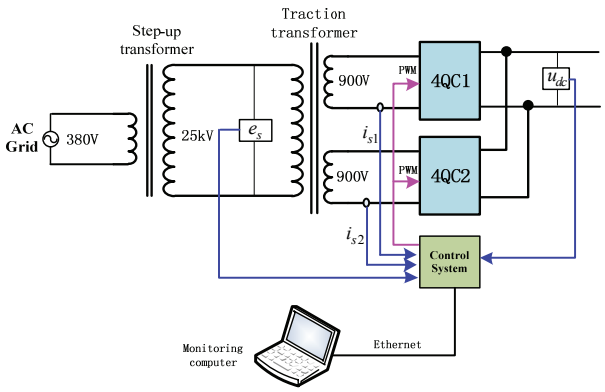

(a)

(b)

Fig. 17. 4QC prototype and test platform: (a) Schematic diagram; (b) Instruments and equipment.

VI. Experimental Verification

A. Prototype and Test Platform

The proposed predictive current control scheme is verified on a newly developed 4QC prototype test platform as shown in Fig. 17. This platform includes a step-up transformer, a traction transformer, two 4QCs, a control system and a monitoring computer. The parameters of 4QC1 and 4QC2 are shown in Table I. Two 4QCs are connected in parallel at the DC side. 4QC1 has two control loops. The inner loop is the current loop, and outer loop is the DC voltage loop which keeps the DC voltage constant. 4QC2 only has a current loop, and the current reference i_{d2}^{*} can be given by the monitoring computer. If 4QC2 works at the rectifying state, 4QC1 works at the inverting state, and the energy can circulate through the two converters. In this test platform, the capacity of the AC grid is 400kVA.

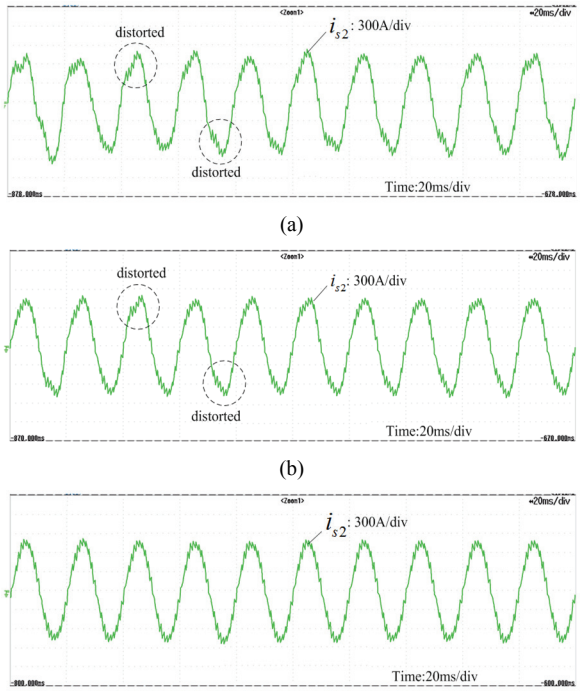

(a)

(b)

(c)

Fig. 18. Experimental waveforms of the prototype with different control methods: (a) Conventional method T_d=T_s; (b) Conventional method T_d=0.5T_s; (c) Predictive current control.

The control system is based on a "DSP+FPGA" framework. The DSP completes the key control algorithm, and the FPGA takes charge of communication and logical control. The monitoring computer is connected to the control system by means of Ethernet. Therefore, the data transmission and state monitoring can be realized.

B. Steady Performance

Fig. 18 shows full-load experimental waveforms of the prototype with different control methods. i_{s2} is the actual AC current waveform of 4QC2. It can be seen from Fig.18 that when T_d=T_s, an obvious distortion can be found in the current waveform (marked by dashed circle). It can also be seen that when T_d=0.5T_s, the distortion in the current waveform is attenuated. When the predictive current control is adopted, the distortion becomes smaller.

In addition, it can be found from the experiments that the current loop can easily become unstable if the control parameters (e.g. kp, ki) of the current loop are increased when T_d=0.5T_s. On the other hand, the stability of the current loop is enhanced significantly when the predictive current control is adopted.

Fig. 19 shows the actual sampled value and predicted value of the AC current, which were obtained by the monitoring computer from the control system via Ethernet. It can be seen from Fig. 19 that the predicted value is nearly equal to the actual sampled value. However, the time advances by 0.5T_s.

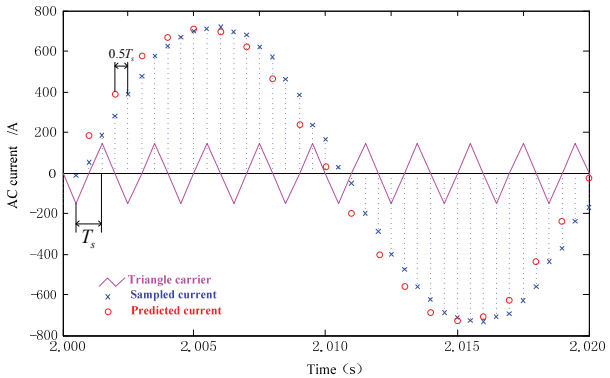

Fig. 19. Sampled current and predicted current of 4QC.

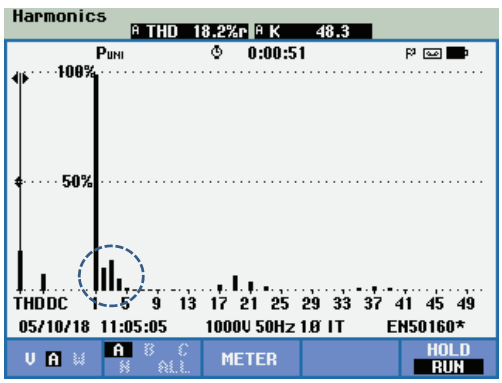

(a)

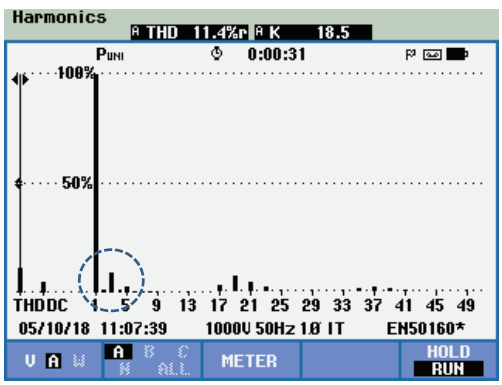

(b)

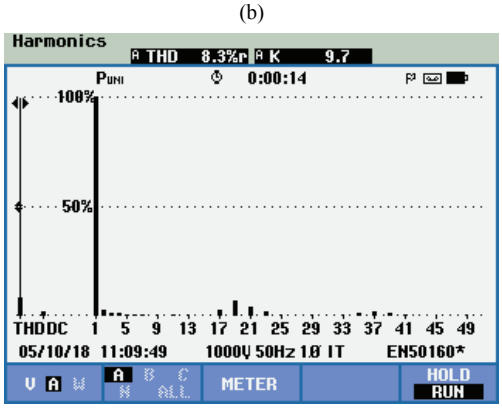

(c)

Fig. 20. Current THD of 4QC under different control methods: (a) Conventional method T_d=T_s; (b) Conventional method T_d=0.5T_s; (c) Predictive current control.

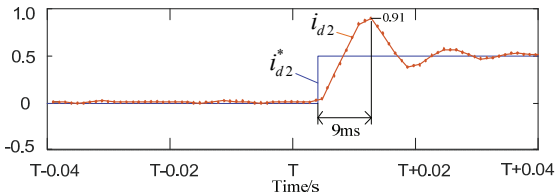

(a)

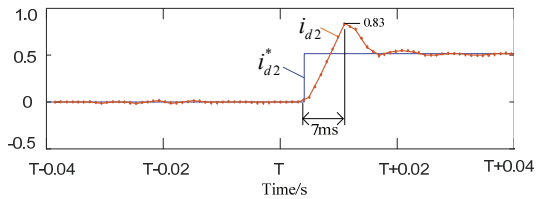

(b)

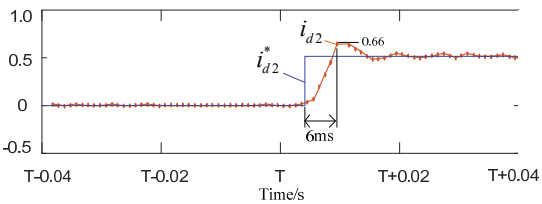

(c)

Fig. 21. Transient responses of 4QC with different control methods: (a) Conventional method T_d=T_s; (b) Conventional method T_d=0.5T_s; (c) Predictive current control.

C. THD

The current THDs of a 4QC with different control methods are shown in Fig. 20. FFT analysis results show that the main characteristic harmonics of the current exist at the orders of 17, 19, 21 and 23 when the unipolar asymmetrical SPWM is employed. These harmonics are not affected by T_d, and can be eliminated through phase-shifted carrier PWM technology [27]. Meanwhile, a large control delay leads to a lot of low order harmonics such as 2, 3, 4 and 5, which are marked with a dashed circle in Fig. 20(a). When T_d=T_s, the current THD is as high as 18.2%. The current THD goes down with a decrease of T_d. Considering the sampling and control algorithm execution time, T_d cannot be reduced to zero with the conventional control method. However, T_d should be close to zero for the proposed predictive current control, and it is shown in Fig. 20(c) that the current THD is reduced to 8.3%.

D. Transient Response

In this paper, the transient response of 4QC with different control methods is evaluated by dynamic loading tests. The current reference i^*_{d2} of 4QC2 is set by the monitoring computer, and then the actual current i_{d2} is transmitted back to the monitoring computer through Ethernet. The data refresh rate of the actual current is 1ks/s.

The current reference i^*_{d2} of 4QC2 increases from 0 to 0.5 (from the no-load to half-load condition) at t=T, and the corresponding current transient response curves are plotted in Fig. 21. It can be seen from Fig. 21 that the rise time is 9ms for T_d=T_s, 7ms for T_d=0.5T_s, and 6ms for the predictive

current control. This means that the computation delay T_d has some impact on the response speed. However, it is not serious. It is worth noting that the computation delay T_d has a dramatic impact on the overshot and settling time. Sudden changes of the load may lead to unacceptable overshoots or even system corruption. The proposed predictive current control demonstrates better transient performance than the conventional control method.

VII. CONCLUSIONS

For a 4QC with a high power and a low switching frequency, the influence of a control delay is especially serious. In this paper, this control delay and its influence are analyzed, and a predictive current control method based on the specific sampling method and the modified z-transform is proposed. Simulation and experimental results both with and without the predictive current control are compared. The following conclusions have been obtained.

(1) The control delay has a negative impact on the system performance of 4QC. With an increase of the control delay, the step response and stability of the system get worse.

(2) The proposed specific sampling method can obtain the fundamental values of the AC current and avoid high frequency harmonic noise.

(3) The proposed predictive current control scheme can effectively waken the influence of the control delay, which improves the current quality and transient responses. Moreover, it is not sensitive to the object model or parameters of 4QC.

The control performance of the proposed predictive current control under complex load and complex grid conditions needs to be studied in the future.

ACKNOWLEDGMENT

This research was funded by the Fundamental Research Funds for the Central Universities (2018JBZ004).

REFERENCES

[1] H. C. Chiang, T. T. Ma, Y. H. Cheng, J. M. Hang, and W. N. Chang, "Design and implementation of a hybrid regenerative power system combining grid-tie and uninterruptible power supply functions," *IET Renew. Power Gener.*, Vol. 4, No. 1, pp. 85-99, Jan. 2010.

[2] Y. J. Gu, Y. X. Wang, W. H. Li, and X. N. He, "Improved virtual vector control of single-phase inverter based on unified model," *IEEE Trans. Energy Convers.*, Vol. 29, No. 3, pp. 611-618, Sep. 2014.

[3] J. Rocabert, A. Luna, F. Blaabjerg, and P. Rodríguez, "Control of power converters in AC microgrids," *IEEE Trans. Power Electron*, Vol. 27, No. 11, pp. 4734-4749, Nov. 2012.

[4] W. Song, S. Jiao, Y. W. Li, J. Wang, and J. Huang, "High-frequency harmonic resonance suppression in high-speed railway through single-phase traction converter with LCL filter," *IEEE Trans. Transport. Electrific.*, Vol. 2, No. 3, pp. 347-356, Sep. 2016.

[5] B. Bahrani and A. Rufer, "Optimization-based voltage support in traction networks using active line-side converters," *IEEE Trans. Power Electron.*, Vol. 28, No. 2, pp. 673-685, Feb. 2013.

[6] L. He, J. Xiong, H. Ouyang, P. Zhang, and K. Zhang, "High-performance indirect current control scheme for railway traction 4QCs," *IEEE Trans. Ind. Electron.*, Vol. 61, No. 12, pp. 6645-6654, Dec. 2014.

[7] D. S. Yang, X. B. Ruan, and H. Wu, "A real-time computation method with dual sampling mode to improve the current control performance of the LCL-type grid-connected inverter," *IEEE Trans. Ind. Electron.*, Vol. 62, No. 7, pp. 4563-4572, Jul. 2015.

[8] C. Zou, B. Liu, S. Duan, and R. Li, "Influence of delay on system stability and delay optimization of grid-connected inverters with LCL filter," *IEEE Trans. Ind. Informat.*, Vol. 10, No. 3, pp. 1775-1784, Aug. 2014.

[9] S. Bibian and H. Jin, "Time delay compensation of digital control for DC switch mode power supplies using prediction techniques," *IEEE Trans.Power Electron.*, Vol. 15, No. 5, pp. 835-842, Sep. 2000.

[10] T. Nussbaumer, M. L. Heldwein, G. H. Gong, S. D. Round, and J. W. Kolar, "Comparison of prediction techniques to compensate time delays caused by digital control of a three-phase buck-type PWM rectifier system," *IEEE Trans. Ind. Electron.*, Vol. 55, No. 2, pp. 791-799, Feb. 2008.

[11] K. Ahmed, A. Massoud, S. Finney, and B. Williams, "Sensor-less current control of three-phase inverter-based distributed generation," *IEEE Trans. Power Del.*, Vol. 24, No. 2, pp. 919-929, Apr. 2009.

[12] Z. Song, C. Xia, and T. Liu, "Predictive current control of three-phase grid-connected converters with constant switching frequency for wind energy systems," IEEE Trans. Ind. Electron., Vol. 60, No. 6, pp. 2451-2464, Jun. 2013.

[13] D. Pan, X. Ruan, C. Bao, W. Li, and X. Wang, "Capacitor-current-feedback active damping with reduced computation delay for improving robustness of LCL-type grid-connected inverter," *IEEE Trans. Power Electron.*, Vol. 29, No. 7, pp. 3414-3427, Jul. 2014.

[14] N. Hoffmann, F. W. Fuchs, M. P. Kazmierkowski, and D. Schröder, "Digital current control in a rotating reference frame - Part I: System modeling and the discrete time-domain current controller with improved decoupling capabilities," *IEEE Trans. Power Electron.*, Vol. 31, pp. 5290-5305, Jul. 2016.

[15] X. Zhang, J. W. Spencer, and J. M. Guerrero, "Small-signal modeling of digitally controlled grid-connected inverters with LCL filters," *IEEE Trans. Ind. Electron.*, Vol. 60, No. 9, pp. 3752-3765, Sep. 2013.

[16] S. Mariéthoz and M. Morari, "Multisampled model predictive control of inverter systems: A solution to obtain high dynamic performance and low distortion," *2012 IEEE Energy Conversion Congress and Exposition (ECCE)*, pp. 1692-1697, 2012.

[17] L. Corradini, W. Stefanutti, and P. Mattavelli, "Analysis of multi-sampled current control for active filters," *IEEE Trans. Ind. Appl.*, Vol. 44, No. 6, pp. 1785-1794, Nov. 2008,

[18] S. N. Vukosavić, L. S. Perić, and E. Levi, "A three-phase digital current controller with improved performance indices," *IEEE Trans. Energy Convers.*, Vol. 32, No. 1, pp. 184-193, Mar. 2017.

[19] S. N. Vukosavic, S. L. Peric, and E. Levi, "AC current controller with error-free feedback acquisition system," *IEEE Trans. Energy Convers*., Vol. 31, No. 1, pp. 381-391, Mar. 2016.
[20] H. Deng, R. Oruganti, and D. Srinivasan, "PWM methods to handle time delay in digital control of a UPS inverter," *IEEE Power Electron. Lett*., Vol. 3, No. 1, pp. 1-6. 2005,
[21] M. Semasa, T. Kato, and K. Inoue, "A simple and effective time delay compensation method for grid-connected inverter with an LCL filter: Application to active damping method," *Control and Modeling for Power Electronics (COMPEL) 2017 IEEE 18th Workshop on*, pp. 1-7, 2017.
[22] C. Chen, J. Xiong, Z. Q. Wan, J. Lei, and K. Zhang, "A time delay compensation method based on area equivalence for active damping of an LCL-type converter," *IEEE Trans. Power Electron*., Vol. 32, No. 1, pp. 762-772, Jan. 2017.
[23] X. Zhang, P. Chen, C. Z. Yu, F. Li, H. T. Do, and R. X. Cao, "Study of a current control strategy based on multisampling for high-power grid-connected inverters with an LCL filter," *IEEE Trans. Power Electron*., Vol. 32, No. 7, pp. 5023-5034, Jul. 2017.
[24] E. I. Jury, *Theory and Application of the Z-Transform Method*, Krieger Publishing Company, Chap. 3, pp. 54-60, 1982.
[25] M. A. Abusara and S. M. Sharkh, "Digital control of a three-phase grid connected inverter," *Int. J. Power Electron*., Vol, 3, No. 3, 299-319, Apr. 2011.
[26] G. Zhang, J. L. Qian, and X. Y. Zhang, "Application of a high-power reversible converter in a hybrid traction power supply system," *Appl. Sci*., Vol. 7, No. 3, 282, Mar. 2017.
[27] B. Li, R. Yang, G. Wang, W. Wang, and D. Xu, "Analysis of the phase-shifted carrier modulation for modular multilevel converters," *IEEE Trans. Power Electron*., Vol. 30, No. 1, pp. 279-310, Jan. 2015.

Gang Zhang was born in Chongqing, China. He received his B.S. and Ph.D. degrees from the School of Electrical Engineering, Beijing Jiaotong University, Beijing, China, in 2005 and 2010, respectively. From 2010 to 2012, he worked as a Post-Doctoral Researcher at Tsinghua University, Beijing, China, where he was engaged in research on high power grid-connected power converters. He is presently working as a Lecture in the School of Electrical Engineering, Beijing Jiaotong University. His current research interests include power electronics and control, high power traction power converters, grid-connected inverters, and energy-saving techniques in subways.

Jianglin Qian was born in Chongqing, China. He received his B.S. and M.S. degrees from the School of Electrical Engineering, Beijing Jiaotong University, Beijing, China, in 2015 and 2017, respectively. Since 2017, he has been working for CRRC Zhuzhou Locomotive Co., Ltd. His current research interests include DC-DC converters and PWM inverter systems.

Zhigang Liu was born in Shandong, China. He received his B.S. and Ph.D. degrees from the School of Electrical Engineering, Beijing Jiaotong University, Beijing, China, in 1986 and 1994, respectively. He is presently working as a Professor in the School of Electrical Engineering, Beijing Jiaotong University. His current research interests include AC drives, traction power supply systems, power electronic circuits and systems, computer network communications, and industrial automation technology.

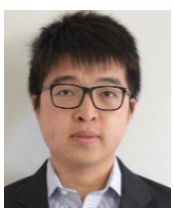

Zhongbei Tian received his B.S. degree from the Huazhong University of Science and Technology, Wuhan, China, in 2013; and his B.S. and Ph.D. degrees in Electrical and Electronic Engineering from the University of Birmingham, Birmingham, ENG, UK, in 2013 and 2017, respectively. He is presently working as a Research Fellow at the University of Birmingham. His current research interests include railway traction systems, power network modeling, energy systems optimization, advanced power systems design, and the analysis of electric railways.